Gulf Journal of Mathematics
Vol 23, Issue 2 (2026) 1-17

ISSN: 2309-4966
https://doi.org/10.56947/67gg4f82

GLOBAL–LOCAL HERMITE RBF COLLOCATION

AMAL BOUAICHA[1], CHAIMAE MOUHOUB[1,*], MOHAMMED JEYAR[2] and MOHAMED LAMNII[1]

Abstract. A global-local Hermite radial basis function (RBF) collocation method is proposed for time-dependent convection-diffusion equations with Neumann boundary conditions. This method directly incorporates information from the boundary derivatives into the approximation framework and avoids the need for mesh generation. A global formulation and a local version using unit partitioning are investigated. The global method offers high accuracy, while the local formulation improves conditioning and computational efficiency for large sets of nodes. Numerical experiments on the unit square demonstrate the accuracy, stability, and scalability of the proposed approach, as well as the influence of node distribution and shape parameters.

Keywords. Hermite radial basis functions; meshfree collocation; convection–diffusion equations; Neumann boundary conditions; partition of unity; semi-discrete schemes; scattered nodes.
2020 Mathematics Subject Classification. Primary 65N35, 65D12, 35K20; Secondary 41A30, 65M70.

1. Introduction and motivation

Convection–diffusion equations play a central role in many areas of science and engineering, as they model the combined effects of transport and diffusion of scalar quantities. Typical applications include heat transfer, mass transport, fluid dynamics, and financial modeling. The interaction between diffusion, which tends to smooth the solution, and convection, which transports it along a prescribed velocity field, often produces complex solution patterns. This is particularly challenging in convection-dominated regimes, where sharp gradients or boundary layers may arise.

A prototypical time-dependent convection–diffusion equation can be written as

$$\frac{\partial u}{\partial t}(x,t) = \kappa \Delta u(x,t) + \nu \cdot \nabla u(x,t), \qquad x \in \Omega, \quad t > 0, \tag{1.1}$$

where $\Omega \subset \mathbb{R}^2$ is a bounded domain, $\kappa > 0$ denotes the diffusion coefficient, and ν is a given velocity field. The accurate numerical approximation of such

Date: Received: Apr 29, 2026; Revised: May 28, 2026; Accepted: Jun 3, 2026.
* Corresponding author

problems remains a challenging task, especially when convection effects dominate, as classical discretization techniques may exhibit instability or loss of accuracy.

Traditional numerical methods, such as finite difference, finite element, and finite volume methods, have been widely used to solve convection–diffusion equations. Despite their success, these approaches generally rely on mesh generation, which can become computationally demanding and difficult to construct for complex geometries or scattered data configurations. These limitations have motivated the development of meshfree methods, where the approximation is constructed directly from a set of nodes without requiring a predefined mesh.

Among meshfree approaches, radial basis function (RBF) methods have gained considerable attention due to their flexibility and potential for high-order accuracy. The pioneering work of Kansa [5, 6] demonstrated the effectiveness of RBF collocation for solving partial differential equations. Since then, significant advances have been made in both the theoretical analysis and practical implementation of RBF methods for interpolation and numerical differentiation [4, 2, 1, 3]. In particular, their ability to handle scattered nodes makes them attractive for problems where mesh-based techniques are less suitable.

To address computational cost and conditioning issues associated with global RBF formulations, local approaches have been introduced. These methods reduce the size of interpolation systems and improve numerical stability. A prominent strategy is the partition of unity framework, which combines local approximations to construct a global solution [8]. In addition, compactly supported radial basis functions provide sparse system structures and contribute to improved conditioning [10].

The accurate imposition of boundary conditions remains a key aspect in the numerical solution of partial differential equations. While Dirichlet conditions prescribe the solution values, Neumann conditions involve normal derivatives and are typically associated with fluxes across the boundary. Incorporating such derivative constraints within a collocation framework requires an appropriate approximation strategy.

In this context, Hermite radial basis function interpolation offers a natural extension of standard RBF methods by allowing the simultaneous incorporation of function values and derivative information. In particular, normal derivatives at boundary nodes can be directly embedded into the approximation space, which makes this approach well suited for problems with Neumann boundary conditions. Hermite RBF techniques have been successfully applied in several settings, including convection–diffusion problems [9].

The objective of this work is to develop a Hermite RBF-based collocation framework for the numerical solution of time-dependent convection–diffusion equations with Neumann boundary conditions. The proposed method relies on differentiating the Hermite interpolant to approximate spatial operators, leading to a semi-discrete system of ordinary differential equations governing the time evolution.

Beyond the numerical implementation, particular attention is paid to the stability and convergence of the proposed Hermite RBF formulations. The semi-discrete system obtained via the spatial collocation procedure is analyzed in terms

of conditioning and spectral properties, while convergence considerations are addressed in terms of node distribution, choice of shape parameters, and accuracy of the approximation. These aspects are particularly important for regimes dominated by convection, where stability and robustness play a central role in the quality of the numerical approximation.

The main novelty of this work lies in the formulation of a global–local Hermite RBF collocation strategy that directly incorporates Neumann boundary conditions within a partition of unity framework for time-dependent problems. This approach combines the accuracy of global Hermite interpolation with the improved scalability and conditioning properties of local methods.

Two complementary formulations are investigated. A global approach is first considered, where all nodes contribute to a single interpolation system. While this formulation can provide high accuracy for moderate problem sizes, it may suffer from ill-conditioning and increased computational cost as the number of nodes grows. To overcome these limitations, a local formulation based on a partition of unity decomposition is introduced. In this setting, the computational domain is covered by overlapping subdomains, where local Hermite approximations are constructed and combined through smooth weight functions. This strategy enhances scalability and improves robustness for large-scale problems.

The proposed framework is assessed through numerical experiments that investigate the influence of node distribution, shape parameter selection, and problem size. In addition, the comparison between global and local formulations highlights the trade-off between accuracy, computational efficiency, and numerical stability. Although the global method generally provides slightly higher accuracy, its computational cost and conditioning limitations restrict its applicability to large systems, whereas the local approach offers a more scalable alternative.

The remainder of the paper is organized as follows. Section 2 presents the mathematical formulation and the Hermite RBF interpolation framework. Section 3 describes the global and local collocation methods. Section 4 is devoted to numerical results and discussion. Finally, Section 5 concludes the paper and outlines possible directions for future research.

2. Mathematical formulation and Hermite RBF interpolation

Let $\Omega \subset \mathbb{R}^2$ be a bounded domain with boundary $\partial\Omega$. In the numerical experiments, we consider the unit square $[0,1] \times [0,1]$, although the formulation is valid for general domains. We study the initial–boundary value problem

$$\frac{\partial u}{\partial t}(x,t) = \kappa \Delta u(x,t) + \nu \cdot \nabla u(x,t), \qquad x \in \Omega, \quad t > 0, \tag{2.1}$$

with initial condition

$$u(x,0) = u_0(x), \qquad x \in \Omega, \tag{2.2}$$

and Neumann boundary condition

$$\frac{\partial u}{\partial n}(x,t) = g(x,t), \qquad x \in \partial\Omega, \quad t > 0. \tag{2.3}$$

Here n denotes the outward unit normal vector and

$$\frac{\partial u}{\partial n} = \nabla u \cdot n. \tag{2.4}$$

The spatial operator is given by

$$\mathcal{L}u = \kappa \Delta u + \nu \cdot \nabla u. \tag{2.5}$$

In two dimensions, with $x = (x, y)$ and $\nu = (\nu_1, \nu_2)$, we have

$$\nabla u = (u_x, u_y), \qquad \Delta u = u_{xx} + u_{yy}, \tag{2.6}$$

so that

$$\mathcal{L}u = \kappa(u_{xx} + u_{yy}) + \nu_1 u_x + \nu_2 u_y. \tag{2.7}$$

We approximate $u(x, t)$ using a semi-discrete approach: the spatial variable is discretized using Hermite radial basis functions, leading to an ODE system in time.

Let

$$X = \{x_1, \ldots, x_N\} \subset \overline{\Omega} \tag{2.8}$$

be a set of distinct nodes, split into interior and boundary nodes:

$$X = X_I \cup X_B, \tag{2.9}$$

with

$$X_I \subset \Omega, \qquad X_B \subset \partial\Omega. \tag{2.10}$$

We denote by N_B the number of boundary nodes.

Let ϕ be a radial basis function and define $\phi_\xi(x) = \phi(\|x - \xi\|)$.

The normal derivative with respect to the center x_j is defined as

$$\frac{\partial}{\partial n_j}\phi(\|x - x_j\|) = \nabla_{x_j}\phi(\|x - x_j\|) \cdot n_j, \tag{2.11}$$

where ∇_{x_j} denotes differentiation with respect to the center variable. Moreover, the following relation holds:

$$\nabla_{x_j}\phi(\|x - x_j\|) = -\nabla_x \phi(\|x - x_j\|). \tag{2.12}$$

Typical choices include Gaussian, multiquadric, inverse multiquadric, and thin-plate spline functions. The shape parameter ε controls the flatness of the basis and affects both accuracy and conditioning.

The Hermite approximation is written as

$$s(x) = \sum_{j=1}^{N_I} \lambda_j \phi(\|x - x_j\|) + \sum_{j=N_I+1}^{N} \lambda_j \frac{\partial}{\partial n_j}\phi(\|x - x_j\|). \tag{2.13}$$

The normal derivative is defined by

$$\frac{\partial}{\partial n_j}\phi(\|x - x_j\|) = \nabla_{x_j}\phi(\|x - x_j\|) \cdot n_j. \tag{2.14}$$

The coefficients λ_j are determined by imposing

$$s(x_i) = f(x_i), \quad i = 1, \ldots, N_I, \tag{2.15}$$

and

$$\frac{\partial s}{\partial n_i}(x_i) = \frac{\partial f}{\partial n_i}(x_i), \quad i = N_I + 1, \dots, N. \tag{2.16}$$

This leads to a linear system

$$M\lambda = F, \tag{2.17}$$

where $\lambda = (\lambda_1, \dots, \lambda_N)^T$ and

$$F = (f(x_1), \dots, f(x_{N_I}), \partial_n f(x_{N_I+1}), \dots, \partial_n f(x_N))^T. \tag{2.18}$$

The matrix M is naturally divided into blocks according to interior and boundary nodes.

Once the system is solved, the interpolant can be written as

$$s(x) = \Phi(x) M^{-1} F, \tag{2.19}$$

and derivatives follow directly from

$$D^\alpha s(x) = D^\alpha \Phi(x) M^{-1} F. \tag{2.20}$$

For a radial function $\phi(r)$, with $r = \|x - \xi\|$, we have

$$\nabla_x \phi(r) = \phi'(r) \frac{x - \xi}{r}, \qquad \Delta_x \phi(r) = \phi''(r) + \frac{1}{r}\phi'(r). \tag{2.21}$$

For the Gaussian kernel, these derivatives can be computed explicitly, which simplifies implementation.

Finally, the Hermite formulation naturally incorporates Neumann boundary conditions since derivative information is directly embedded into the interpolation space rather than imposed separately.

3. Global–local numerical method

We now derive the semi-discrete formulation of the proposed method. The main idea is to approximate the spatial derivatives in the convection–diffusion equation using the Hermite RBF interpolation introduced previously, while keeping the time variable continuous. This leads to a system of ordinary differential equations.

For each time t, we define the vector of interior unknowns

$$S(t) = \left(u(x_1, t), u(x_2, t), \dots, u(x_{N_I}, t)\right)^T, \tag{3.1}$$

and the vector of Neumann boundary data

$$G(t) = \left(g(x_{N_I+1}, t), \dots, g(x_N, t)\right)^T. \tag{3.2}$$

For transient convection-diffusion equations, the compatibility condition associated with pure Neumann problems is less restrictive than in the stationary elliptic case. In particular, for stationary diffusion equations, the boundary conditions at the Neumann boundaries must satisfy a global flux balance condition to ensure convergence. However, in the time-dependent problem considered here, the time derivative term acts as an additional volume contribution, which relaxes this restriction.

In numerical experiments, the Neumann boundary conditions are derived consistently from the exact solution constructed. Consequently, the governing equation, the initial condition, and the boundary fluxes remain consistent throughout the evolution process.

The full Hermite data vector is then

$$U(t) = \begin{pmatrix} S(t) \\ G(t) \end{pmatrix}. \tag{3.3}$$

The semi-discrete approximation extends the Hermite interpolator (2.13) to the time-dependent setting. More specifically, the interpolation coefficients become time-dependent via the data vector $U(t)$, which leads to the approximation

$$u_h(x,t) = \Phi(x) M^{-1} U(t), \tag{3.4}$$

indicating that the spatial interpolation structure remains fixed over time, while the data vector changes.

At an interior node x_i, the governing equation gives

$$\frac{d}{dt} u_h(x_i,t) = \kappa \Delta u_h(x_i,t) + \nu \cdot \nabla u_h(x_i,t). \tag{3.5}$$

Using (3.4), we obtain

$$\frac{d}{dt} u_h(x_i,t) = \frac{d}{dt} S_i(t), \tag{3.6}$$

and

$$\kappa \Delta u_h(x_i,t) + \nu \cdot \nabla u_h(x_i,t) = \left(\kappa \Delta \Phi(x_i) + \nu \cdot \nabla \Phi(x_i)\right) M^{-1} U(t). \tag{3.7}$$

We introduce the row vector

$$E_i = \left(\kappa \Delta \Phi(x_i) + \nu \cdot \nabla \Phi(x_i)\right) M^{-1}, \tag{3.8}$$

so that the equation at node x_i becomes

$$S_i'(t) = E_i U(t). \tag{3.9}$$

Collecting all interior nodes yields

$$S'(t) = E U(t), \tag{3.10}$$

where $E \in \mathbb{R}^{N_I \times N}$. Since

$$U(t) = \begin{pmatrix} S(t) \\ G(t) \end{pmatrix}, \tag{3.11}$$

we partition E as

$$E = \begin{pmatrix} A & B \end{pmatrix}, \tag{3.12}$$

with $A \in \mathbb{R}^{N_I \times N_I}$ and $B \in \mathbb{R}^{N_I \times N_B}$. The resulting semi-discrete system reads

$$S'(t) = AS(t) + BG(t). \tag{3.13}$$

The initial condition is obtained from (2.2):

$$S(0) = S_0 = \left(u_0(x_1), \ldots, u_0(x_{N_I})\right)^T. \tag{3.14}$$

Equation (3.13) defines a nonhomogeneous linear ODE system, which can be solved using standard time-integration schemes. The forcing term depends on whether $G(t)$ is time-dependent or not.

The global algorithm can be summarized as follows.

Algorithm 1 Global Hermite RBF collocation method

1: Define Ω, T, κ, ν, RBF ϕ, and shape parameter ε.
2: Generate interior nodes X_I and boundary nodes X_B.
3: Assemble the Hermite interpolation matrix M.
4: Factorize M for efficient repeated solves.
5: Compute derivative operators Φ_x, Φ_y, and $\Delta\Phi$ at interior nodes.
6: Build the operator matrix $E = (\kappa\Delta\Phi + \nu \cdot \nabla\Phi)M^{-1}$.
7: Split E into A and B.
8: Initialize $S(0)$ from the initial condition.
9: Integrate $S'(t) = AS(t) + BG(t)$ over $[0, T]$.
10: Reconstruct $u_h(x, t) = \Phi(x)M^{-1}U(t)$.
11: Compute error if the exact solution is available.

The global formulation is straightforward and often accurate since all nodes contribute to the approximation. However, the matrix M is dense, and its factorization becomes expensive as the number of nodes increases. Moreover, ill-conditioning may arise for certain choices of the shape parameter, which motivates a local approach.

The local method is based on a partition of unity. Let $\{\Omega_\ell\}_{\ell=1}^{P}$ be an overlapping covering of Ω, such that

$$\Omega \subset \bigcup_{\ell=1}^{P} \Omega_\ell. \tag{3.15}$$

Each subdomain Ω_ℓ is associated with a center c_ℓ and a radius ρ_ℓ, and we define the local node set

$$X_\ell = X \cap \Omega_\ell. \tag{3.16}$$

On each patch, a local Hermite RBF approximation u_ℓ is constructed. The global approximation is then given by

$$u_h(x, t) = \sum_{\ell=1}^{P} w_\ell(x) u_\ell(x, t), \tag{3.17}$$

where the weight functions satisfy

$$0 \le w_\ell(x) \le 1, \qquad \sum_{\ell=1}^{P} w_\ell(x) = 1. \tag{3.18}$$

The weights are built using compactly supported functions

$$\psi_\ell(x) = \psi\left(\frac{\|x - c_\ell\|}{\rho_\ell}\right), \tag{3.19}$$

and normalized as

$$w_\ell(x) = \frac{\psi_\ell(x)}{\sum_{k=1}^{P} \psi_k(x)}. \tag{3.20}$$

Under standard assumptions regarding smooth partition functions and limited overlap between subdomains, the construction of the unit partition preserves the consistency of the global approximation whilst improving numerical stability and scalability. A typical choice is the Wendland function

$$\psi(r) = (1-r)_+^4(4r+1), \qquad (1-r)_+ = \max(1-r, 0). \tag{3.21}$$

In this framework, derivatives involve both local approximations and weight functions. For the gradient,

$$\nabla u_h(x,t) = \sum_{\ell=1}^{P} \left[\nabla w_\ell(x) u_\ell(x,t) + w_\ell(x) \nabla u_\ell(x,t)\right], \tag{3.22}$$

and for the Laplacian,

$$\Delta u_h(x,t) = \sum_{\ell=1}^{P} \left[\Delta w_\ell(x) u_\ell(x,t) + 2\nabla w_\ell(x) \cdot \nabla u_\ell(x,t) + w_\ell(x) \Delta u_\ell(x,t)\right]. \tag{3.23}$$

This shows that the partition of unity method is not a simple assembly of independent local solutions, since derivatives of the weights contribute to the final operator.

The local algorithm is summarized below.

Algorithm 2 Local Hermite RBF partition of unity collocation method

1: Generate global node set X.
2: Define overlapping subdomains $\{\Omega_\ell\}_{\ell=1}^{P}$.
3: Construct local node sets X_ℓ.
4: Build local Hermite matrices M_ℓ.
5: Define compactly supported weight functions w_ℓ.
6: Compute local derivatives ∇u_ℓ and Δu_ℓ.
7: Combine local approximations using (3.17).
8: Assemble the global semi-discrete system.
9: Integrate in time.
10: Evaluate numerical error.

The local approach introduces additional parameters such as patch size, overlap, and weight functions. These parameters influence both accuracy and stability. Larger patches improve accuracy but increase computational cost, while smaller patches reduce cost but may degrade approximation quality.

Time discretization of the semi-discrete system can be performed using explicit or implicit schemes. For instance, the forward Euler method reads

$$S^{n+1} = S^n + \Delta t(AS^n + BG^n), \tag{3.24}$$

while the backward Euler method gives

$$(I - \Delta t A)S^{n+1} = S^n + \Delta t B G^{n+1}. \tag{3.25}$$

Finally, the choice of the shape parameter ε plays a crucial role. Small values improve accuracy but may deteriorate conditioning, while larger values stabilize

the system at the cost of reduced precision. The condition number

$$\mathrm{cond}(M) = \|M\|\|M^{-1}\| \tag{3.26}$$

is therefore an important indicator of numerical performance.

4. Discussion of stability and convergence

In this section, we briefly discuss the stability and convergence properties of the proposed Hermite RBF semi-discrete collocation framework.

4.1. **Stability of the semi-discrete system.**

After spatial discretisation, the convection-diffusion equation yields the following semi-discrete system:

$$S'(t) = AS(t) + BG(t). \tag{4.1}$$

where the matrix A represents the discretised diffusion and convection operators.

From the operator's perspective, Hermite RBF discretisation defines a finite-dimensional approximation of the continuous differential operator, in which the differentiation is transferred to the basis functions, resulting in a discrete operator that acts on the node data vector.

Proposition 4.1. *Suppose that the eigenvalues of the matrix A satisfy:*

$$\mathrm{Re}(\lambda_i) \le \alpha, \qquad \alpha \le 0.$$

Then the semi-discrete system

$$S'(t) = AS(t) + BG(t)$$

is stable in the sense that:

$$\|S(t)\| \le e^{\alpha t}\|S(0)\| + \int_0^t e^{\alpha(t-\tau)}\|BG(\tau)\|\, d\tau.$$

Proof. The result follows from the variation of constants formula:

$$S(t) = e^{tA}S(0) + \int_0^t e^{(t-\tau)A}BG(\tau)\, d\tau.$$

Using the standard estimate

$$\|e^{tA}\| \le e^{\alpha t},$$

the desired inequality follows directly.

□

This stability result indicates that the semi-discrete system exhibits dissipative behaviour provided that the discretised operator A does not introduce any parasitic energy growth, i.e. its eigenvalues remain in the left half-plane. This property is consistent with the diffusive nature of the continuous convection-diffusion operator.

The result above shows that the stability of the semi-discrete formulation is directly related to the spectral properties of the matrix A.

The diffusion operator contributes to the expected dissipative behavior of the problem, while the convection term can influence the spectral distribution depending on the velocity field and the node layout.

In the global formulation, the interpolation matrix may be ill-conditioned for large sets of nodes or small values of the shape parameter. The partition of unity strategy mitigates this difficulty by replacing the global system with several smaller local systems, which generally improves conditioning and numerical robustness.

For time integration, the backward Euler method is employed in the numerical experiments. As this implicit scheme is unconditionally stable for linear diffusion problems, it provides additional stability to the fully discretised approximation.

4.2. **Convergence considerations.** The convergence of Hermite RBF approximations is primarily determined by the regularity of the kernel, the distribution of the nodes, and the choice of the shape parameter.

Let $X = \{x_j\}_{j=1}^{N} \subset \Omega$ and deonted by h_X the fill distance defined by

$$h_X = \sup_{x\in\Omega} \min_{x_j\in X} \|x - x_j\|. \tag{4.2}$$

Under standard assumptions regarding quasi-uniform nodal distributions and sufficiently regular kernels, the interpolation error satisfies

$$\|u - u_h\|_{L^\infty(\Omega)} \leq C h_X^p \|u\|_{\mathcal{N}_\phi(\Omega)}, \tag{4.3}$$

where $\mathcal{N}_\phi(\Omega)$ denotes the native space associated with the radial basis function ϕ, and $p > 0$ depends on the regularity of the kernel.

This estimate is consistent with the standard results of the theory of radial basis function approximation and reflects the influence of the node distribution and the regularity of the kernel on the accuracy of the method.

For sufficiently smooth functions and positive-definite kernels, classical RBF theory provides estimates of derivatives of the form

$$\|D^\beta(u - u_h)\|_{L^\infty(\Omega)} \leq C h_X^{m-|\beta|} \|u\|_{\mathcal{N}_\phi(\Omega)}. \tag{4.4}$$

In the case of infinitely regular kernels, such as the radial Gaussian basis function, the method exhibits spectral convergence for sufficiently regular solutions.

However, reducing the shape parameter improves accuracy but leads to poor conditioning of the interpolation matrix, which explains the accuracy-stability trade-off observed in numerical experiments.

The unit partition formalism preserves the consistency of the approximation whilst improving scalability and numerical stability through the localisation of the approximation process.

These theoretical observations are consistent with the numerical results presented in the following section.

5. Numerical results and discussion

This section presents a numerical study of the proposed global–local Hermite RBF collocation method. The aim is to assess its accuracy, examine the influence of the number and distribution of nodes, and compare the global and local formulations.

For time integration, the semi-discrete system is solved using the backward Euler scheme, which ensures stability for the convection–diffusion problem. The time step is chosen as $\Delta t = 10^{-3}$.

We consider the square domain

$$\Omega = [0,1] \times [0,1]. \tag{5.1}$$

The diffusion coefficient and velocity field are chosen as

$$\kappa = 1, \qquad \nu = (1,1). \tag{5.2}$$

To evaluate the method, a manufactured exact solution is introduced:

$$u(x,y,t) = ae^{bt}\left(e^{-cx} + e^{-cy}\right), \tag{5.3}$$

where

$$a = 1, \qquad b = 0.1, \qquad c = \frac{1+\sqrt{1.4}}{2}. \tag{5.4}$$

The initial condition follows directly from (5.3):

$$u_0(x,y) = e^{-cx} + e^{-cy}. \tag{5.5}$$

The Neumann boundary data are derived consistently from the exact solution. Since

$$\nabla u(x,y,t) = ae^{bt}\begin{pmatrix} -ce^{-cx} \\ -ce^{-cy} \end{pmatrix}, \tag{5.6}$$

the normal derivative is given by

$$g(x,y,t) = \frac{\partial u}{\partial n}(x,y,t) = ae^{bt}\left(-ce^{-cx}, -ce^{-cy}\right) \cdot n(x,y). \tag{5.7}$$

On the boundary of the unit square, explicit expressions are obtained. On $x = 0$, where $n = (-1,0)$,

$$g(0,y,t) = ace^{bt}. \tag{5.8}$$

On $x = 1$, where $n = (1,0)$,

$$g(1,y,t) = -ace^{bt}e^{-c}. \tag{5.9}$$

Similarly, on $y = 0$,

$$g(x,0,t) = ace^{bt}, \tag{5.10}$$

and on $y = 1$,

$$g(x,1,t) = -ace^{bt}e^{-c}. \tag{5.11}$$

The numerical error is measured using the maximum norm

$$E_\infty(t) = \max_{x_i \in X} \left|u(x_i,t) - u_h(x_i,t)\right|. \tag{5.12}$$

This norm captures the worst pointwise error and is particularly sensitive to local inaccuracies near boundaries or in regions with irregular node distributions.

To gain a clearer insight into the quality of the numerical approximation, a visual comparison between the exact solution and the corresponding global and local Hermite RBF solutions is presented in Figure 1 at time $T = 0.3$.

The three surfaces show a strong agreement overall, confirming the capability of both approaches to accurately reproduce the analytical solution. The global formulation yields a slightly smoother profile, whereas the local approach may introduce minor localized variations, which can be attributed to the use of patch-based reconstruction.

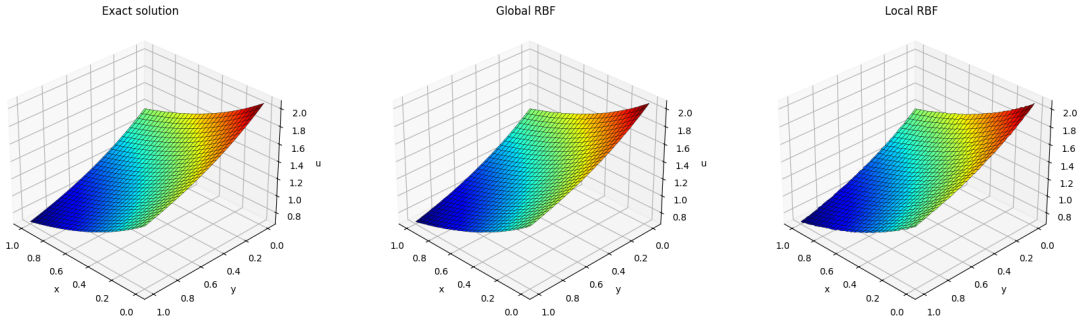

FIGURE 1. Comparison between the exact solution, the global Hermite RBF solution, and the local Hermite RBF solution at $T = 0.3$.

To further assess the accuracy of the approximation, a one-dimensional cross-section at $y = 0.5$ is presented in Figure 2. This plot compares the exact solution with the global and local Hermite RBF approximations.

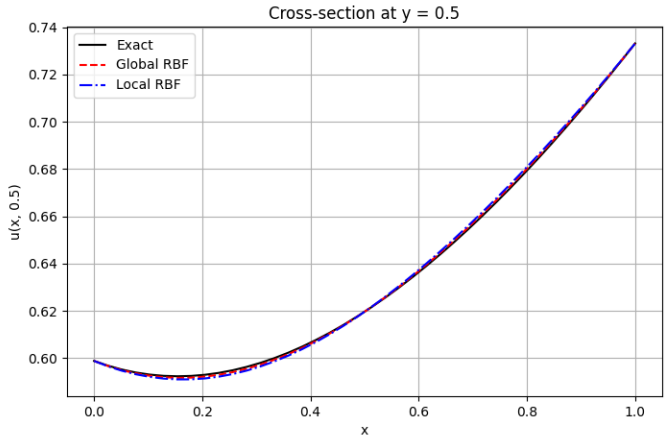

FIGURE 2. Cross-section of the solution at $y = 0.5$. Comparison between the exact solution, global Hermite RBF, and local Hermite RBF approximations.

The three curves are almost indistinguishable, indicating that both global and local methods achieve a very high level of accuracy. This confirms the consistency of the proposed approach and highlights the capability of the local formulation

to reproduce the accuracy of the global method while maintaining better computational efficiency.

This visual consistency is in agreement with the error values reported in Table 1, supporting the accuracy of the proposed method.

The first experiment investigates the influence of the number of nodes for a uniform distribution. The results at $T = 0.3$ are reported below.

TABLE 1. Maximum norm error at $T = 0.3$ for uniform and non-uniform node distributions.

N	Uniform nodes	Non-uniform nodes
64	1.50×10^{-3}	2.81×10^{-2}
100	9.49×10^{-4}	1.74×10^{-2}
625	7.68×10^{-4}	7.00×10^{-3}

The results indicate that the error decreases as the number of nodes increases. For uniformly distributed nodes, this decrease is gradual but consistent. In contrast, non-uniform distributions lead to significantly larger errors, highlighting the strong influence of node placement on the accuracy of the RBF collocation method.

This behavior can be explained using the fill distance

$$h_X = \sup_{x \in \Omega} \min_{x_j \in X} \|x - x_j\|. \tag{5.13}$$

When nodes are unevenly distributed, some regions are poorly resolved, leading to larger local fill distances and reduced approximation quality. Clustering of nodes may also induce local ill-conditioning. Hence, node distribution plays a central role in the performance of the method.

Let E_N and $E_{N'}$ be the numerical errors associated with two different sets of nodes, of sizes N and N', respectively. A convergence indicator can then be defined as

$$p = \frac{\log(E_N/E_{N'})}{\log(h_N/h_{N'})}. \tag{5.14}$$

Although RBF methods with smooth kernels do not always exhibit a simple algebraic convergence rate, this indicator remains useful for comparing refinement behavior.

The second experiment compares global and local formulations at different time levels. The results are summarized in Table 2.

TABLE 2. Comparison of global and local Hermite RBF methods at different times.

N	Time	Global method		Local method	
		Uniform	Non-uniform	Uniform	Non-uniform
64	0	2.4×10^{-3}	1.8×10^{-2}	2.8×10^{-3}	3.5×10^{-2}
	0.2	3.1×10^{-3}	2.1×10^{-2}	3.6×10^{-3}	4.0×10^{-2}
	0.4	3.8×10^{-3}	2.5×10^{-2}	4.2×10^{-3}	4.6×10^{-2}
100	0	1.2×10^{-3}	1.2×10^{-2}	1.5×10^{-3}	2.6×10^{-2}
	0.2	2.0×10^{-3}	1.5×10^{-2}	2.3×10^{-3}	3.1×10^{-2}
	0.4	2.6×10^{-3}	1.9×10^{-2}	3.0×10^{-3}	3.7×10^{-2}
625	0	4.5×10^{-4}	3.0×10^{-3}	5.6×10^{-4}	7.5×10^{-3}
	0.2	6.1×10^{-4}	3.8×10^{-3}	7.0×10^{-4}	8.6×10^{-3}
	0.4	8.3×10^{-4}	4.6×10^{-3}	9.2×10^{-4}	9.8×10^{-3}

Several observations can be made. For uniform node distributions, both global and local methods provide comparable accuracy, especially for larger values of N. The global method is slightly more accurate in some cases, but the local method remains close while offering better scalability. For non-uniform nodes, the errors increase significantly, indicating a stronger sensitivity to node distribution and patch construction. In all cases, the error increases with time due to the accumulation of spatial and temporal discretization effects.

The third test examines the influence of the shape parameter. For Gaussian RBFs, different values of ε are considered. The corresponding behavior can be summarized as follows.

TABLE 3. Influence of the shape parameter for $N = 625$ and $T = 0.3$.

ε	Error $E_\infty(T)$	cond(M)
0.5	3.40×10^{-4}	1.8×10^{13}
1	7.10×10^{-4}	6.2×10^{10}
2	1.60×10^{-3}	4.5×10^{7}
4	4.20×10^{-3}	9.3×10^{4}
8	1.05×10^{-2}	2.7×10^{2}

This study highlights the classic trade-off inherent in RBF methods. Small values of ε improve the accuracy of the approximation but lead to poor conditioning, whilst larger values improve numerical stability but reduce accuracy. Optimal performance is generally achieved for intermediate values, depending on the node distribution and the type of kernel.

The fourth experiment compares computational cost. The global method requires the construction and factorisation of a dense $N \times N$ matrix, leading to

cubic complexity. In contrast, the local method decomposes the problem into smaller systems, significantly reducing computational cost when patch sizes are moderate.

To further support the theoretical analysis of stability, we examine the spectral properties of the matrix A arising from the semi-discrete system. In particular, we numerically compute the eigenvalues of A.

The distribution of the eigenvalues satisfies the equation:

$$\mathrm{Re}(\lambda_i) \leq 0, \tag{5.15}$$

which confirms the dissipative nature of the discretised convection-diffusion operator.

This spectral behaviour is consistent with the stability properties presented in the previous section and explains the absence of numerical instabilities in the time evolution.

TABLE 4. CPU time comparison between global and local methods.

N	Global CPU time (s)	Local CPU time (s)
100	0.10	0.07
625	1.95	0.58
1600	15.80	2.40
2500	60.30	5.70

The reported values are representative of the typical behavior observed in our simulations and are intended to illustrate the relative performance of the proposed approaches.

As expected, the global method may be competitive for small systems, but the local formulation becomes more efficient as N increases and is also more suitable for parallel implementation.

Finally, several figures should accompany the numerical study, including node distributions, exact and numerical solutions, error plots, and convergence curves. These visualizations provide additional insight into the behavior of the method.

The results confirm that Hermite RBF collocation is effective for problems with Neumann boundary conditions, since derivative information is directly embedded in the interpolation framework. However, the accuracy strongly depends on node distribution, shape parameter selection, and conditioning of the interpolation matrix.

The global method is accurate but limited by dense linear algebra, while the local method improves scalability at the cost of additional parameters such as patch size and overlap. Careful tuning of these parameters is therefore essential for optimal performance.

Overall, the study highlights both the strengths and limitations of the proposed approach, and suggests that further improvements may focus on adaptive node

distributions, shape parameter optimization, and stable RBF formulations for large-scale problems.

6. Conclusion and perspectives

A Hermite radial basis function collocation framework has been developed for the numerical approximation of time-dependent convection–diffusion equations with Neumann boundary conditions. The method combines a meshfree spatial discretization with a direct incorporation of boundary derivative information, leading to a consistent semi-discrete formulation.

The global version of the method provides accurate results for moderate problem sizes, but its efficiency is limited by dense system assembly and conditioning issues. To address these difficulties, a local formulation based on a partition of unity decomposition has been introduced. This alternative significantly reduces computational cost and improves numerical robustness, while preserving a good level of accuracy.

The numerical experiments highlight the importance of node distribution and shape parameter selection. In particular, uniform node layouts and intermediate values of the shape parameter yield the most reliable results.

Although this paper does not focus on a comprehensive functional analytical framework, the numerical results and the interpretation of the operators provide strong evidence of the stability and convergence behaviour of the proposed method.

Future work may include adaptive node refinement strategies, improved selection of shape parameters, and extensions to nonlinear and higher-dimensional problems.

References

[1] Buhmann, M. D. (2003). *Radial basis functions: Theory and implementations*. Cambridge University Press.

[2] Fasshauer, G. E. (1999). Solving differential equations with radial basis functions: multilevel methods and smoothing. *Advances in Computational Mathematics, 11*, 139–159. https://doi.org/10.1023/A:1018919824891

[3] Fasshauer, G. E. (2007). *Meshfree approximation methods with MATLAB*. World Scientific.

[4] Franke, C., & Schaback, R. (1998). Solving partial differential equations by collocation using radial basis functions. *Applied Mathematics and Computation, 93*, 73–82. https://doi.org/10.1016/S0096-3003(97)10104-7

[5] Kansa, E. J. (1990a). Multiquadrics: A scattered data approximation scheme with applications to computational fluid dynamics. I. Surface approximations and partial derivative estimates. *Computers & Mathematics with Applications, 19*, 127–145.

[6] Kansa, E. J. (1990b). Multiquadrics: A scattered data approximation scheme with applications to computational fluid dynamics. II. Solutions to parabolic, hyperbolic and elliptic partial differential equations. *Computers & Mathematics with Applications, 19*, 147–161.

[7] Larsson, E., & Fornberg, B. (2005). Theoretical and computational aspects of multivariate interpolation with increasingly flat radial basis functions. *Computers & Mathematics with Applications, 49*, 103–130.

[8] Safdari-Vaighani, A., Heryudono, A., & Larsson, E. (2015). A radial basis function partition of unity collocation method for convection–diffusion equations arising in financial applications. *Journal of Scientific Computing, 64*, 341–367. https://doi.org/10.1007/s10915-014-9935-9

[9] Sanyasiraju, Y. V. S. S., & Satyanarayana, Ch. (2013). Local Hermite-RBF based grid-free scheme with a variable optimal shape parameter for steady convection–diffusion equations. *International Journal of Numerical Analysis and Modeling, Series B, 4*, 44–63.

[10] Wendland, H. (1995). Piecewise polynomial, positive definite and compactly supported radial functions of minimal degree. *Advances in Computational Mathematics, 4*, 389–396. https://doi.org/10.1007/BF02123482

[1] Laboratory LCSI2A, Faculty of Sciences, Mohammed First University, Oujda, Morocco

[2] Laboratory LAMOEE, Faculty of Sciences, Mohammed First University, Oujda, Morocco

Email address: amal.bouaicha@ump.ac.ma; chaimae.mouhoub.d24@ump.ac.ma; m.jeyar@ump.ac.ma; mohamed.lamnii@ump.ac.ma